Dipo: a miniaturized hopping robot via lightweight and compact actuator design for power amplification

IOP Publishing Bioinspir. Biomim. 18 (2023) 046006 https://doi.org/10.1088/1748-3190/acd290

Bioinspiration & Biomimetics

PAPER

RECEIVED
15 December 2022

REVISED
1 May 2023

ACCEPTED FOR PUBLICATION
4 May 2023

PUBLISHED
16 May 2023

Dipo: a miniaturized hopping robot via lightweight and compact actuator design for power amplification

Chan Kim[1], **Dong-Jun Lee**[1], **Sun-Pill Jung**[2] **and Gwang-Pil Jung**[1,*]

[1] Department of Mechanical and Automotive Engineering, Seoul National University of Science and Technology, Seoul 01811, Republic of Korea

[2] School of Mechanical and Aerospace Engineering/Institute of Advanced Machines and Design, Seoul National University, Seoul 151-742, Republic of Korea

[*] Author to whom any correspondence should be addressed.

E-mail: gpjung@seoultech.ac.kr

Keywords: bio-inspired robot, hopping robot, jumping robot, active clutch, power spring

Supplementary material for this article is available online

Abstract

Kangaroo rats are well known as representative hoppers in small-scale animals. Especially kangaroo rats show rapid movement when a predator approaches. If this amazing motion can be applied to small-scale robots, they will be able to traverse lands at high speed while overcoming size limitations. To take advantage of hopping locomotion, in this paper, we present a lightweight and small-scale clutch-based hopping robot called Dipo. To make this possible, a compact power amplifying actuation system has been developed using a power spring and an active clutch. The power spring is possible to take out and use the accumulated energy little by little whenever the robot starts to hop. Moreover, the power spring needs low torque to charge the elastic energy, and a only tiny space is required to install. The active clutch controls the motion of hopping legs by adjusting the timing of energy release and storage. Thanks to these design strategies, the robot weighs 45.07 g, has the height of 5 cm in the stance phase, and achieves the maximum hopping height of 54.9 cm.

1. Introduction

A kangaroo rat is a one of the representative examples of small animals that perform hopping. They are simply known for good hoppers but in fact, they sometimes use their legs as a means of performing other purposeful motion. In ordinary times, *Dipodomys deserti*, a kangaroo rat species, leaps at an average horizontal distance of 0.28 m (two body length) and a vertical height of 0.15 m (one body length) (Best *et al* 1989, Schwaner *et al* 2021). When kangaroo rats meet predators, however, they use high acceleration for avoidance (Freymiller *et al* 2017, Rankin *et al* 2018). At this time, they can jump about nine times higher than the hip position with a maximum vertical jump height of 0.4 m (Rankin *et al* 2018, Schwaner *et al* 2018). If this amazing locomotion is applied to the actual centimeter-scale robots, it can dramatically increase the robot's mobility by using the concept of vertical hopping.

Until now, many small robots have been developed that can jump intermittently. For meaningful intermittent jumping, the process of storing and releasing a large amount of energy needs to be required. To this end, a parallel-elastic linkage has been mostly employed to amplify the electric motor's limited power (Lambrecht *et al* 2005, Kovač *et al* 2009, Li *et al* 2012, Nguyen and Park 2012, Zhao *et al* 2013, Woodward and SITTI 2014, Zaitsev *et al* 2015, Jung *et al* 2016, 2019, Bai *et al* 2018, Li and Rus 2019, Hong *et al* 2020, Chae *et al* 2022, Hawkes *et al* 2022, Shin *et al* 2022).

For example, Hawkes *et al* introduce a device that can jump over 30 meters high (Hawkes *et al* 2022). The device uses the concept of work multiplication. By using a ratcheted motor and a releasing mechanism, the energy is stored in elastic materials

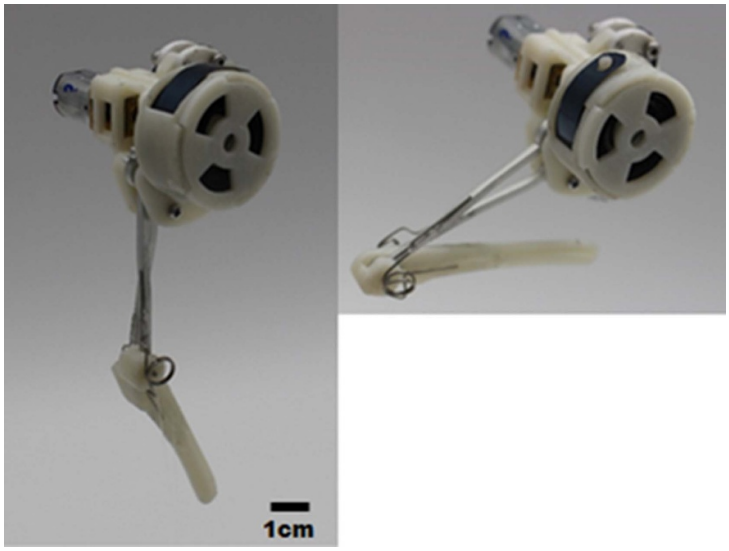

Figure 1. A miniaturized hopping robot. The Dipo has the height of 5 cm in the stance phase and weight of 45.07 g.

and is released at take-off. Zhao *et al* achieves steerable jumping and self-righting via a single DC motor (Zhao *et al* 2013). The robot uses a one-way bearing to store the elastic energy by deforming the body structure. Energy is releases when the one-way bearing passes the critical position. In a result, the robot jumps 87 cm in vertical height. Those intermittently jumping robots have shown excellent jumping performance. However, they require quite a long time to restore the elastic energy for the next jump, which has the potential to deteriorate agility and maneuverability. To resolve the issue, hopping locomotion has been actively studied for small-scale robots to enable them to move faster over lands while overcoming their size limitations.

As the scale of the hopping robots gets small, however, it is hard to achieve high power actuation. In case of electromagnetic motors which is well known for their high torque property, for example, the torque is dependent with the gap radius of the motor (Seok *et al* 2012). In other words, the torque decreases in proportional to the square of the gap radius. To amplify the motors' limited power, the power amplification mechanism varies depending on the connection method between the elastic components and the motors. The power amplification mechanisms for small hopping robots based on motors and elastic components are as follows: (a) a series-elastic actuator (De and Koditschek 2015, Haldane *et al* 2016b) and (b) a parallel-elastic actuator (Batts *et al* 2016a, Lee *et al* 2021).

De *et al* introduce a 2 kg bipedal robot having passive-compliant legs and an active inertial tail. The robot is hip-driven and a brushless motor is located at each hip. The leg is serially connected to the hip. The leg is composed of a four-bar linkage with a linear spring inside the linkage for leg compliance. For the hopping locomotion, the hip motor controls the leg touchdown angle in the aerial phase and the tail motor adjusts body shape in flight to store the energy into the passive linear spring inside the leg. Consequently, the robot achieves a hopping height of 1.6 times the leg length.

Salto-1P uses two steps of serial-elastic actuation and mechanical advantage (MA) adaptation to amplify the motor's power (Haldane *et al* 2016a, 2016b, Plecnik *et al* 2017, Yim and Fearing 2018). In the first stage where MA is low, the motor deforms the torsional rubber tube and stores the energy. The power output from the motor and the rubber tube is transferred to the specially designed eight-bar linkage. This eight-bar linkage has little MA at the beginning but has substantially large MA at the end. Therefore, the power output from the motor and the rubber tube is extremely amplified in the end. In a result, the robot can continuously jump up to 1.252 m, which is higher than five times of its body length.

REBO hopper employs paper-folded springs and brushless DC motors to load energy into the springs (Chen *et al* 2020). Pulley-borne cables connected to the DC motors pull the springs, and sudden loss of tension releases the spring, generating a 20 W power stroke. In a result, the robot achieves aerial phase apex 25% above the stance height. Batts *et al* from Disney Research use a linear spring as an energy-storing material (Batts *et al* 2016b). To charge the energy, a linear elastic actuator in parallel based on a voice coil actuator is employed to compress and release the spring.

In this paper, we present a lightweight and miniaturized hopping robot, called Dipo shown in figure 1. The Dipo is the first active clutch-based

small-scale hopping robot, which is not tried previously. In general, additional linkage structures are employed for power amplification, which has possibility to increase the size and the weight. To solve the issue, a power spring and an active clutch are used. First of all, the power spring requires only a tiny space to install and is possible to accumulate the elastic energy with low torque. Furthermore, the power spring has a large amount of angular displacement and accordingly, it is easy to take out the accumulated energy little by little to use it. The active clutch controls the timing of energy storage and release. By using these two main components, a compact actuation system has been made and the hopping robot can be miniaturized. The Dipo has the height of 5 cm in the stance phase and achieves the maximum hopping height of 54.9 cm.

In the following sections, design, modeling, and experimental results are stated. The design section describes the working process of the hopping mechanism. The modeling section analyzes the kinematics and dynamics to determine design parameters. In the results section, the mechanism is tested and the corresponding results are given.

2. Design

2.1. Overall design

Figure 2 shows the conceptual design of the Dipo. Basically, the Dipo uses a one degree-of-freedom (DoF) four-bar linkage to realize hopping motion through a single actuator. The four-bar linkage consists of a folding link, a stretching link, and a jumping link. The jumping link directly contacts the ground when the Dipo hops. The folding link and the stretching link are used to fold and stretch the leg. To this end, these links have one gear at the end of the link, respectively.

The gear of the folding link is directly connected to the barrel gear which is the main source for transferring the elastic energy in the power spring. To quickly fold the leg and save the elastic energy in the power spring, the gear ratio between the barrel gear and the folding gear is set as 1:1.

The gear of the stretching link is connected to a compound gear. To transfer the stretching torque to the leg, the compound gear is essential. This compound gear reverses the rotating direction of the barrel gear since the barrel gear rotates only in a clockwise direction. In addition, the compound gear allows us to adjust the gear ratio between the barrel gear and the stretching gear. To magnify the torque, the final gear ratio from the barrel gear to the stretching gear is set as 5.56:1. The detail design of the compound gear is shown in figure 4. The compound gear does not fully rotate and reciprocates within a portion having the gear teeth. The rotating direction of the compound gear is determined by the active clutch.

At the knee of the hopping leg shown in figure 2, a torsion spring is embedded to absorb the impact energy when the Dipo is in the landing phase. The knee spring has the stiffness of 0.8 mNm/° and saves 0.063 J, which is 20% of the energy required for a single jump.

2.2. Power amplifying actuation

To make the 45.07 g hopping robot achieve the average hopping height of 45.33 cm, the final output power of the actuator should be about 9.5 W. Currently, the Dipo's actuator generates about 60 mNm of torque at 1370 rpm and weighs 28.13 g, which is about 9.69 W of the final output power. If we consider high-end brushless DC electric motors (BLDC), the motor (Maxon ECXSP13L, GPX13HS 25:1) requires 60 g of mass to generate equal torque and angular speed.

To get a lightweight but high-power actuator, a power spring is employed as an energy-storing component. The power spring has high torque delivery per unit deflection and is easy to install in tiny spaces due to its compactness. In terms of the torque curve shown in figure 3(a), the power spring shows significant differences compared to a typical torsion spring.

In figure 3(a), both springs have an equal amount of stored energy. The torsion spring has high peak torque and small angular displacement, while the power spring has a relatively low torque but a long angular displacement. So, if the same amount of elastic energy is needed to be stored, only a low-torque motor is enough to fully charge the power spring.

In addition, the power spring provides a nearly constant torque by utilizing the long flatter central section shown in figure 3(a). During the section, the power spring's torque just slightly varies and this easily enables to generate a similar level of torques. Figure 3(b) shows the torque curve of the power spring used for the Dipo. This power spring has about 60 mNm of torque level and about 1800° of the flatter central section.

2.3. Active clutch for hopping timing control

In figure 4, the barrel, the barrel gear, the power spring inside the barrel, and the main motor are connected through a single axis. The motor rotates the power spring and the elastic energy is stored. The active clutch controls the flow of this stored energy. But, making a decision where and when to supply the energy is very important. Depending on the decision, the Dipo may or may not achieve successful hopping.

The active clutch shown in figure 2 determines the flow of energy transfer. Figure 2 shows how the active clutch works (Lee and Jung 2020). In stretching mode, the clutch makes the barrel gear contact to the compound gear. The compound gear transfers the torque to the stretching gear and finally, the Dipo jumps. In folding mode, the barrel gear is moved to the folding

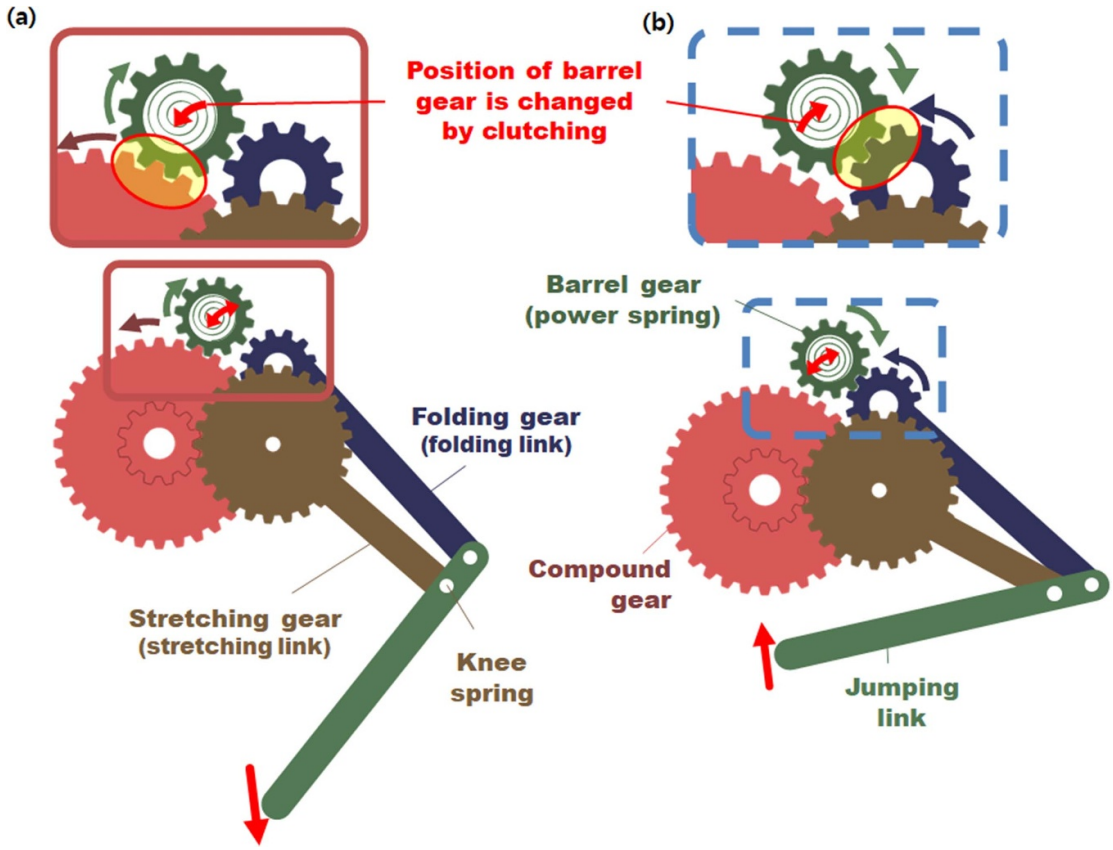

Figure 2. Schematic of the Dipo's clutching mechanism. (a) Stretching mode and (b) folding mode. The barrel gear where the power spring is installed rotates in a single direction. Stretching and folding motion is controlled using the active clutch.

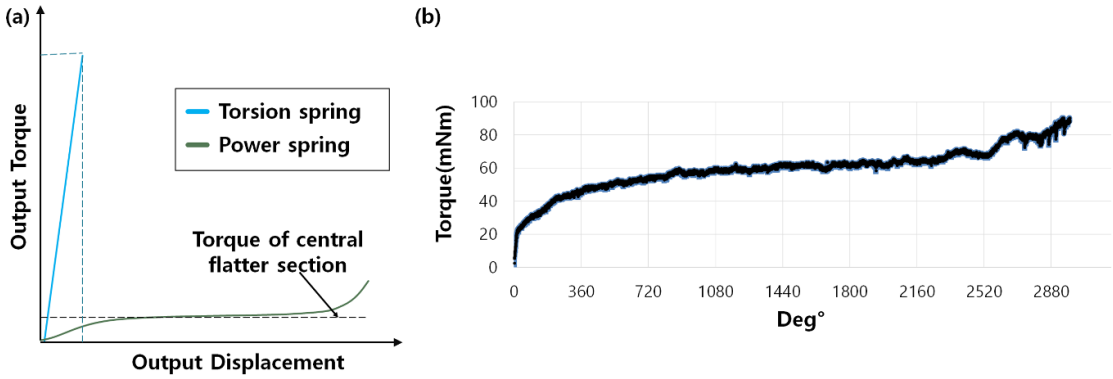

Figure 3. (a) Torque curves of a torsion spring and a power spring. The power spring has long central flatter section. (b) Torque curve of the power spring used for the Dipo. The curve has the central flatter section having the average torque of 60 mNm.

gear by the clutch and the folding link is pulled back as shown in figure 2(b).

Figure 5 shows the working algorithm of the active clutch. The posture of the hopping leg and the amount of the energy stored in the power spring are estimated in real time through two encoders. With information from the encoders, the active clutch determines where and when to supply the stored energy. The Dipo determines the energy release timing based on the encoder installed at the stretching link. The current posture is estimated based on this encoder. When the angle is lower than 30°, it is determined as the time to supply energy to the stretching link.

To make the Dipo hop 45.33 cm continuously, 0.24 J (with guide mass) of elastic energy is required at each jump. This corresponds to 370° of angular displacement of the power spring and it takes 45 ms to transfer the torque. The active clutch controls this duration and the clutching timing simultaneously.

Figures 5(a) and (b) present the clutching process and the corresponding movement, respectively. The

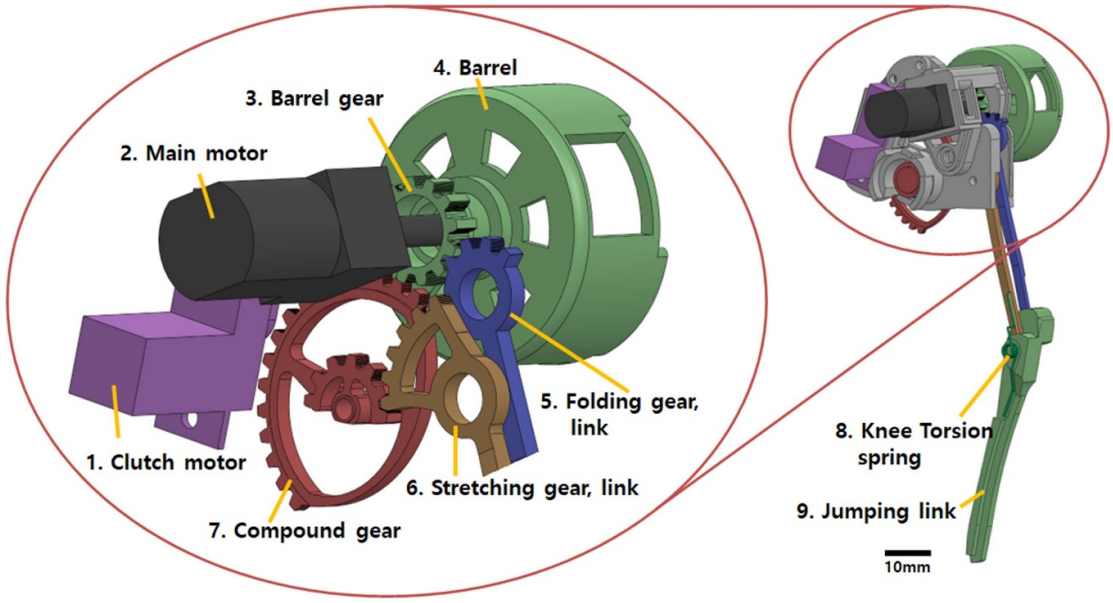

Figure 4. Detail design of the Dipo.

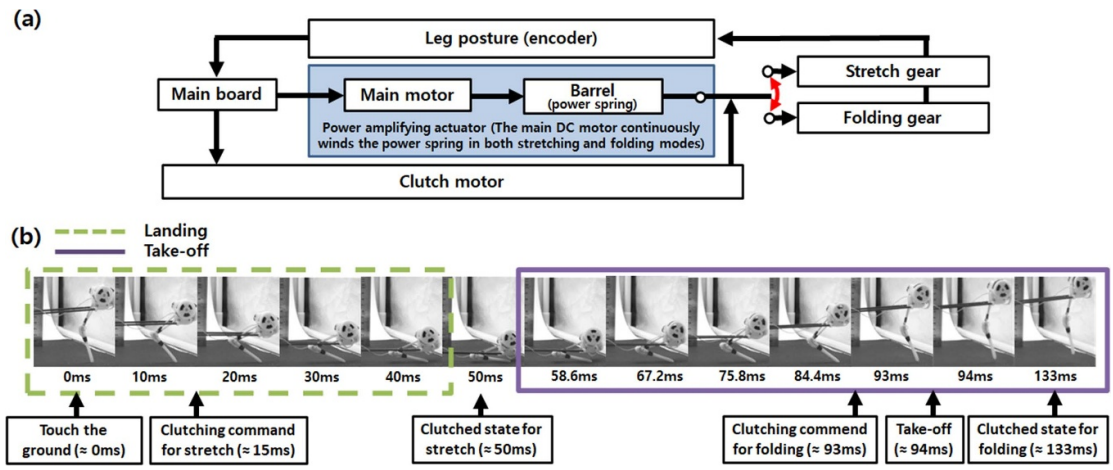

Figure 5. (a) Working process of the active clutch and (b) experiment conducted during the landing to take-off phase.

posture of the leg during hopping is estimated in real time through the encoder. Using this information, the active clutch determines the appropriate timing for releasing the stored energy. Figure 5(b) shows landing and take-off using high-speed images. After the robot lands and the leg contacts the ground, the clutching command is given at about 15 ms, which is before the leg fully folds. This is because there exists about 40 ms delay from the clutching command to the real operation. At 50 ms, the robot is in fully folded state and starts to stretch the leg to take off. The clutching command for folding is given at about 93 ms. The actual operation occurs at about 133 ms, which is after take-off.

2.4. Other components

Mass budget of the Dipo is given in table 1. The Dipo uses a lightweight controller board (Teensy 4.0, PJRC) and a DC motor (200:1, Pololu Inc.). For the active clutch, a miniature servo motor (PDI-DHV56MG) is employed. The hopping leg has a magnetic encoder (EzEnocoder i2A systems Inc.) in its knee and the encoder has a resolution of 0.36°.

Table 1. Mass budget.

Components	Quantity (ea.)	Mass (g)	Mass ratio (%)
Body frame	1	9.53	21.1
Leg	1	2.7	6.0
Stretching gear	1	0.94	2.1
DC motor	1	10.42	23.1
Clutch servo	1	3.43	7.6
Barrel & power spring	1	17.71	39.3
Encoder	1	0.34	0.8
Total		45.07	100.0

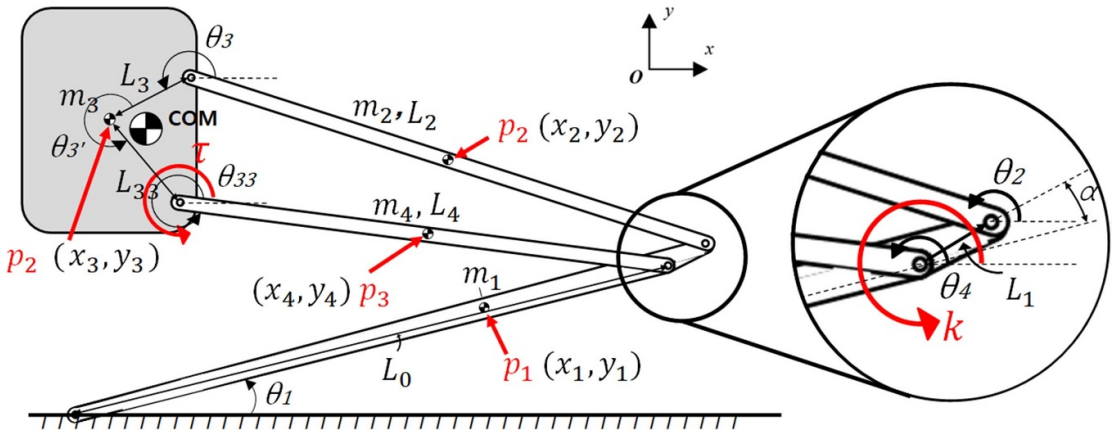

Figure 6. Schematic of the Dipo modeling.

3. Modeling and analysis

Take-off of the Dipo finishes within tens of milliseconds. Therefore, dynamic analysis is essential for us to understand the behavior of the Dipo. Through the analysis, dynamic properties such as the take-off time, velocity, acceleration, and the reaction force are estimated.

In addition, hopping leg optimization is done to choose the design parameters. Determining the parameters of the hopping leg is essential to maximize the take-off speed while preventing unwanted rotation. To this end, the foot trajectory and the take-off speed are investigated by varying the length of the hopping linkage.

3.1. Dynamics

The Dipo is modeled with the four linkages, five joints, the power spring, and the knee spring as shown in figure 6. Currently, the Dipo uses a guide for stable hopping. It is mounted on the body of the robot and prevents rotation. Therefore, the x-coordinate of the body's COM and the body's attitude are kept constant. The dynamic analysis is done using the Lagrangian multiplier (Flores and Lankarani 2016) and the main formulation is as follows:

$$\begin{bmatrix} M_{12\times12} & J^{\mathrm{T}}_{12\times10} \\ J_{10\times12} & O_{10\times10} \end{bmatrix} \begin{bmatrix} \ddot{q}_{12\times1} \\ \lambda_{10\times1} \end{bmatrix} = \begin{bmatrix} g_{12\times1} \\ \gamma_{10\times1} \end{bmatrix} \quad (1)$$

where q is the generalized coordinate, γ is the acceleration vector, g is the external force vector, J is the Jacobian matrix, and λ is the Lagrangian multiplier. The matrix elements are given in appendix.

The initial value of θ_1 and θ_3 have the angle of 7.5° and 153.27°, respectively. Based on the above equations and values, equation (1) is numerical solved using ODE45 function in MATLAB.

3.2. Take-off

Take-off of the jumping mechanism occur when the vertical reaction force, $V(t)$ in equation (2), is zero

$$m_{\mathrm{robot}}a_{\mathrm{robot},y} = \sum_{i=1}^{4} m_i a_{i,y}(t) = V(t) - \sum_{i=1}^{4} m_i g \quad (2)$$

where m_{robot} is the total mass, a_{robot} is the acceleration of the mass center, and a_i is the acceleration of each link.

The take-off translational velocity (equation (3)) are determined as follows:

$$m_{\mathrm{robot}}v_{\mathrm{robot}} = \sum_{i=1}^{6} m_i v_{i,f} \quad (3)$$

where v_{robot} is the velocity of the mass center. $v_{i,f}$ is the translational velocity, and $w_{i,f}$ is the angular velocity of each link just before takeoff.

The visualization of the Dipo during take-off is given in figure 7. It takes 45 ms to take off from the fully folded state. One noticeable point is that the hopping leg is not fully unfolded at the take-off timing. In figure 7(a), θ_3 is 291° while fully unfolded state has 282° of θ_3. This tells us that there exists residual energy in the Dipo and this affects the energy efficiency (Jung *et al* 2014). Based on the posture at the take-off timing, the residual energy is estimated as 0.052 J. Given that the released energy of 0.387 J from the power spring (Calculated energy when using the power spring at 370° in figure 3(b)), the energy efficiency is given as 86.6%. For the cross check, residual energy and the energy efficiency are estimated through the take-off speed.

Figure 8 shows the simulated results of the velocity, acceleration, and reaction force during take-off. The take-off velocity is given as 3.52 m s^{-1}. The take-off acceleration is investigated as 162.7 m s^{-2}, which is 16.6 times greater than the gravitational acceleration.

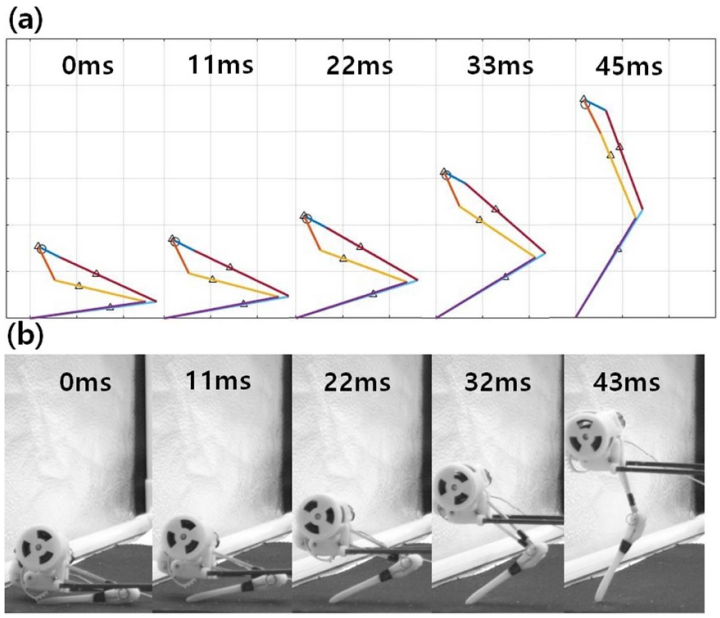

Figure 7. (a) Visualization of the dynamic modeling and (b) high-speed images during take-off.

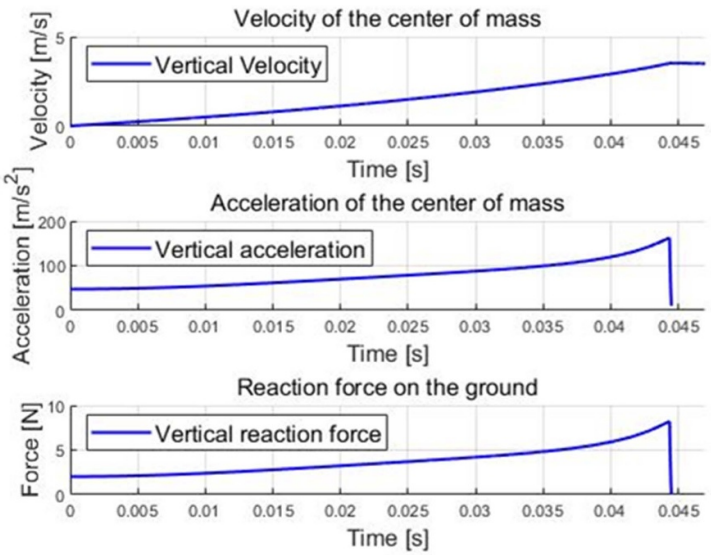

Figure 8. Velocity and acceleration of the robot's center of mass and reaction force from the ground.

The reaction force from the ground shows 8.23 N and this corresponds to 15.8 times of its body weight.

3.3. Hopping linkage analysis

The Dipo uses a 1 DoF four-bar linkage as the hopping leg. To avoid unwanted rotation and to assure stable hopping, the four-bar linkage is designed to fulfill two requirements—a straight line of the foot trajectory and the foot trajectory passing through the mass center. On the other hand, maximizing the take-off velocity is also essential to increase the hopping performance. To satisfy the requirements while maximizing the take-off speed, a parametric study is done based on the dynamic model.

The hopping leg consists of four linkages and each link is indicated as L_0, L_1, L_2, L_3, and L_4. L_0 and L_1 are actually a single linkage but have a bent angle, α, as shown in figure 6. For the optimization, L_2 and L_4 are selected as design variables since these parameters substantially affect the foot trajectory and the take-off speed; to change the L_3 is difficult due to the structural limitation and L_1 is designed as short as possible to increase the angular speed of the hopping leg, L_0.

Figure 9 shows the take-off speed by varying the length of L_2 and L_4. The range of L_2 and L_4 are 43.8–46.8 mm and 39.4–40.7 mm, respectively. To effectively explain the variation of the take-off speed and the foot trajectory, the graph is divided into three

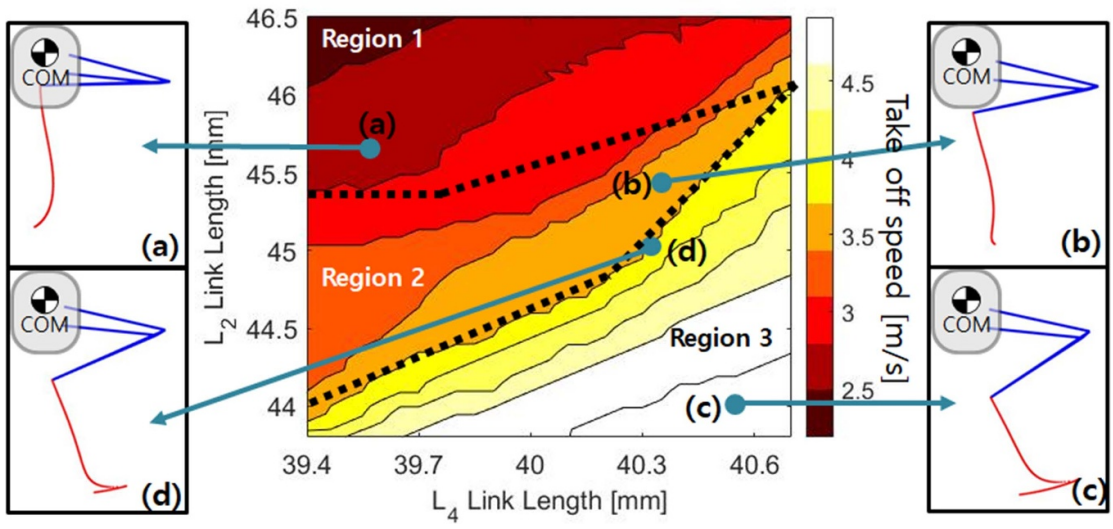

Figure 9. Take-off speed and foot trajectories depending on the length of the links, L_2 and L_4.

regions; the regions are separated using dashed lines in figure 9. In region 1, the foot trajectory has a near straight line and passes through the center of mass as shown in figure 9(a). However, the Dipo is not able to fully fold the leg since the foot crashes into the body structure. In region 3, the foot trajectory is far from the straight line, which causes unstable take-off and landing.

Region 2 satisfies the requirements. The foot trajectory has a near straight line and the line passes through the mass center. Furthermore, the foot does not crash into the body structure when the Dipo is in the fully folded state. If we choose the point (d) located near the borderline to maximize the take-off speed, the foot trajectory cannot be assured as a straight line due to the insufficient margin for error. Therefore, point b in region 2 is selected as the final value. At this point, L_2 and L_4 have 45.31 mm and 40.31 mm, respectively, showing the take-off speed of 3.52 m s^{-1}.

Other design parameters such as the length of L_0 and the angle of α indicated in figure 6 rarely affect the shape of the foot trajectory. These parameters are mainly related with the length and the direction of the foot trajectory. Considering the design requirements, therefore, L_1 and α are determined as 54.72 mm and 259°, respectively.

4. Experimental results

4.1. Model validation

The parametric study is done based on the dynamic analysis and the design parameters are finally chosen as shown in table 2. This selection, however, is valid when the simulation has good agreement with the experimental results. To check whether the simulated results correspond to the actual hopping experiment, the take-off motion of a single hop is precisely observed using the high-speed camera.

Figure 7(b) shows the high-speed images taken with the frame rate of 900 fps. From the pictures, the take-off time, take-off speed and the change in linkage posture are investigated. To begin with, it takes 45 ms to take off in the simulation. This is when the vertical reaction force is zero. In the case of the experiment, the timing when the foot is separated from the ground is observed and the take-off time is given as 45 ms. The take-off time also can be confirmed through figure 10 showing the take-off speed. The take-off speed from the model shows 3.52 m s^{-1} at 45 ms and starts to drop due to gravity. For the experiment, the peak occurs at 43 ms and the take-off speed is given as 3.33 m s^{-1}. After the peak, the speed decreases, similar to the simulation.

Furthermore, variations of the angles such as θ_1 and θ_4 are drawn to check the similarity in posture during take-off. In figures 7(a) and (b), it seems that the visualization of the dynamic model corresponds to the actual jumping of the Dipo. Figure 11 precisely shows the similarity in posture by providing the variation of the angles. Figure 7(a) indicates the angle θ_1 which is between the foot and the ground. In the case of figure 7(b), the angle between the link L_1 and L_4 is drawn to check the shape of the four-bar linkage. In both figures 7(a) and (b), the angle data between the model and the experiment shows good agreement entirely.

4.2. Hopping performance

To investigate the Dipo's performance, hopping experiments are done. Values of the parameters are given in table 2. In figure 12, the Dipo hops using a rotation guide and the hopping motion is observed through a high-speed camera at a rate of 250 fps. In

Table 2. Dimensions of DIPO.

L_1(mm)	L_2(mm)	L_3(mm)	L_4(mm)	L_{11}(mm)	L_{x1}(mm)	L_{x2}(mm)	L_{x4}(mm)	L_{33}(mm)
54.72	45.31	10.64	40.31	50.09	34.67	28.31	10.60	16.25
m_1(g)	m_2(g)	m_3(g)	m_4(g)	m_1(g)	Guide (g)	k(mNm/°)		τ(mNm/°)
1.16	0.71	42.03	0.79	1.16	8.74	0.8		333

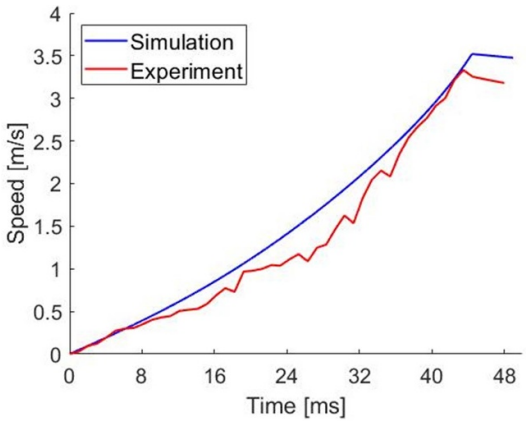

Figure 10. Take-off speed from the model and the experiments.

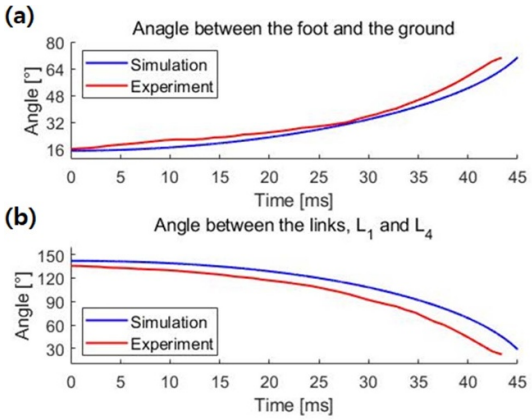

Figure 11. Variation of the angles such as (a) θ_1 and (b) the angle between the links L_1 and L_4.

figure 13, the position of the mass center is drawn depending on the time based on the video analysis. During the 18 jumps, the Dipo shows average hopping height of 45.33 cm and the standard deviation of 4.56 cm. Take-off speed is given as 3.33 m s^{-1} in average. In case of the hopping frequency, a single jump takes 720 ms in average and this indicates the frequency of 1.39 Hz.

In respect of energy transfer, the experiment shows an average mechanical efficiency of 77% at each hop. Compared to the simulated results, the experimental results show a bit lower take-off velocity, hopping height and the mechanical efficiency. The difference may occur because of the mechanical friction between components and the vibration of the guide. In the attached video materials, the guide experiences torsion and bending while the Dipo hops. We estimate that this causes unwanted disturbances and affects to Dipo's hopping performance.

The energy conversion ratio—ratio of electric energy to kinetic energy for a single hop—has been checked. For a single jump, the Dipo needs 0.55 A at a voltage of 7.4 V during 0.6 s and this corresponds to 2.4 J. Based on the Dipo's hopping height, the Dipo has kinetic energy of 0.24 J and therefore, the energy conversion ratio is given as 10%. This seems to be a fair number in that the Salto-1P and the EPFL hopper show 8% (Haldane *et al* 2017) and 9% (Shin *et al* 2022), respectively.

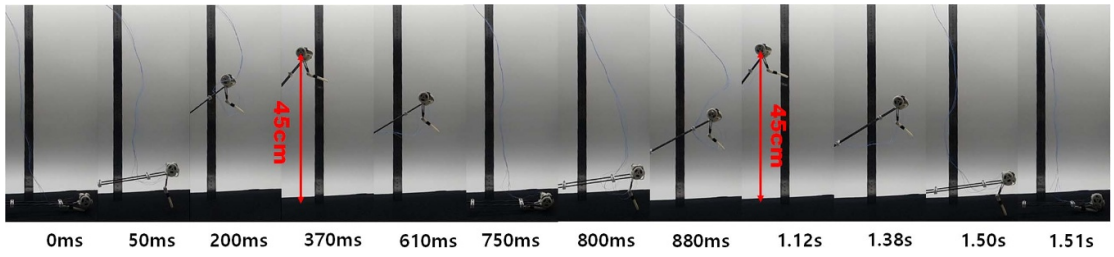

Figure 12. Sequential pictures of the hopping motion.

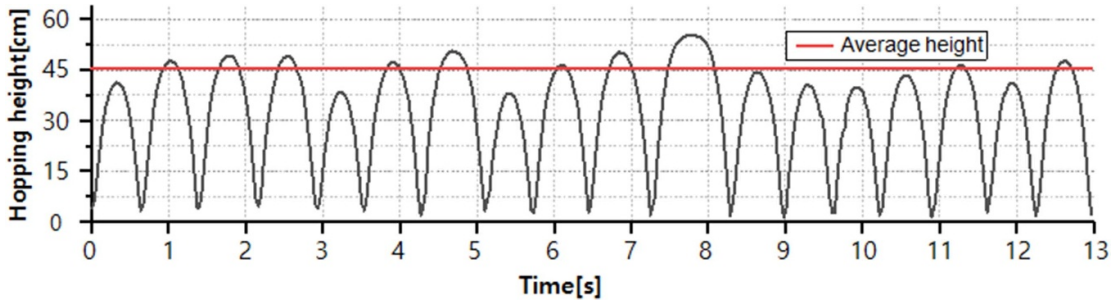

Figure 13. Trajectory of the mass center during 18 hops. The average hopping height is measured as 45 cm.

5. Conclusion

In this paper, we proposed a lightweight and miniaturized hopping robot. The key issue was how to make a power-amplifying actuation system while reducing its mass and volume. To resolve the issue, a power spring and an active clutch have been employed. The power spring enabled the Dipo to continuously generate the torque required to hop. Using the active clutch, the Dipo could release the elastic energy at the right timing. To show the performance of the proposed design, a prototype has been constructed and hopping experiments are done. In a result, the Dipo weighs 45.07 g, has the height of 5 cm in the stance phase, and has an average hopping height of 45.33 cm.

Dipo employs a four-bar linkage mechanism, which poses a significant challenge in terms of generating a smooth and straight trajectory for the legs. This, in turn, leads to the generation of moments that can potentially cause unwanted rotations. To address this issue, we are actively pursuing the development of various techniques such as the utilization of propellers (Haldane *et al* 2017), active tails (An *et al* 2022), and reaction wheels (Ryadchikov *et al* 2018). These methods would help to minimize the impact of moment generation on the robot's body.

Data availability statement

All data that support the findings of this study are included within the article (and any supplementary files).

Acknowledgments

This work was supported by the National Research Foundation of Korea (NRF) Grant funded by the Korean Government (MSIP) (NRF-2022R1F1A1063824). This research was also supported by Korea Institute for Advancement of Technology (KIAT) Grant funded by the Korea Government (MOTIE) (P0008473, HRD Program for Industrial Innovation).

Appendix. The matrix elements

The generalized coordinate vector is as follows:

$$\mathrm{M} = \mathrm{diag}\left[m_1 \;\; m_1 \;\; I_1 \;\; m_2 \;\; m_2 \;\; I_2 \;\; m_3 \;\; m_3 \;\; I_3 \;\; m_4 \;\; m_4 \;\; I_4\right] \tag{4}$$

$$\mathrm{O} = \begin{bmatrix} 0 & \cdots & 0 \\ \vdots & \ddots & \vdots \\ 0 & \cdots & 0 \end{bmatrix}_{11\times 11}. \tag{5}$$

The constraint equations are given as follows:

$$f_1 = -x_1 + L_{x1}\cos\theta_1 = 0$$

$$f_2 = -y_1 + L_{x1}\sin\theta_1 = 0$$

$$f_3 = x_1 + (L_1 - L_{x1})\cos\theta_1 - x_2 + L_{x2}\cos\theta_2 = 0$$

$$f_4 = y_1 + (L_1 - L_{x1})\sin\theta_1 - y_2 + L_{x2}\sin\theta_2 = 0$$

$$f_5 = x_2 + (L_2 - L_{x2})\cos\theta_2 - x_3 + L_3\cos\theta_3 = 0$$

$$f_6 = y_2 + (L_2 - L_{x2})\sin\theta_2 - y_3 + L_3\sin\theta_3 = 0$$

$$f_7 = x_3 + L_{33}\cos(\theta_3 + \theta_{3'}) - x_4 + L_{x4}\cos\theta_4 = 0$$

$$f_8 = y_3 + L_{33}\sin(\theta_3 + \theta_{3'}) - y_4 + L_{x4}\sin\theta_4 = 0$$

$$f_9 = L_{11}\cos(\theta_1 - \alpha) - x_4 + (L_4 - L_{x4})\cos\theta_4 = 0$$

$$f_{10} = L_{11}\sin(\theta_1 - \alpha) - y_4 + (L_4 - L_{x4})\sin\theta_4 = 0$$

$$\alpha = 0.7^\circ.$$

The Jacobian matrix is given and is calculated as follows based on the constraint equations:

$$J = \begin{bmatrix} -1 & 0 & J_{1,3} & 0 & 0 & 0 & 0 & 0 & 0 & 0 & 0 & 0 \\ 0 & -1 & J_{2,3} & 0 & 0 & 0 & 0 & 0 & 0 & 0 & 0 & 0 \\ 1 & 0 & J_{3,3} & -1 & 0 & J_{3,6} & 0 & 0 & 0 & 0 & 0 & 0 \\ 0 & 1 & J_{4,3} & 0 & -1 & J_{4,6} & 0 & 0 & 0 & 0 & 0 & 0 \\ 0 & 0 & 0 & 1 & 0 & J_{5,6} & -1 & 0 & J_{5,9} & 0 & 0 & 0 \\ 0 & 0 & 0 & 0 & 1 & J_{6,6} & 0 & -1 & J_{6,9} & 0 & 0 & 0 \\ 0 & 0 & 0 & 0 & 0 & 0 & 1 & 0 & J_{7,9} & -1 & 0 & J_{7,12} \\ 0 & 0 & 0 & 0 & 0 & 0 & 0 & 1 & J_{8,9} & 0 & -1 & J_{8,12} \\ 0 & 0 & J_{9,3} & 0 & 0 & 0 & 0 & 0 & 0 & 1 & 0 & J_{9,12} \\ 0 & 0 & J_{10,3} & 0 & 0 & 0 & 0 & 0 & 0 & 0 & 1 & J_{10,12} \end{bmatrix} \quad (6)$$

$$J_{1,3} = -L_{x1}\sin\theta_1, J_{2,3} = L_{x1}\cos\theta_1,$$

$$J_{3,3} = -(L_1 - L_{x1})\sin\theta_1, J_{4,3} = (L_1 - L_{x1})\cos\theta_1$$

$$J_{3,6} = -L_{x2}\sin\theta_2, J_{4,6} = L_{x2}\cos\theta_2,$$

$$J_{5,6} = -(L_2 - L_{x2})\sin\theta_2, J_{6,6} = (L_2 - L_{x2})\cos\theta_2$$

$$J_{5,9} = -L_3\sin\theta_3, J_{6,9} = L_3\cos\theta_3,$$

$$J_{7,9} = -L_{33}\sin(\theta_3 + \theta_{3'}), J_{8,9} = -L_{33}\cos(\theta_3 + \theta_{3'})$$

$$J_{7,12} = -L_{x4}\sin\theta_4, J_{8.12} = L_{x4}\cos\theta_4,$$

$$J_{9,12} = -(L_4 - L_{x4})\sin\theta_4, J_{10,12} = (L_4 - L_{x4})\cos\theta_4$$

$$J_{9,3} = L_{11}\sin\theta_1, J_{10,3} = -L_{11}\cos\theta_1$$

where L_{xi} is the distance between the mass center and the Link, L_i.

The generalized coordinate vector is as follows:

$$q^{\mathrm{T}} = \begin{bmatrix} x_1 & y_1 & \theta_1 & x_2 & y_2 & \theta_2 & x_3 & y_3 & \theta_3 & x_4 & y_4 & \theta_4 \end{bmatrix} \quad (7)$$

$$\gamma = \begin{bmatrix} L_{x1}\cos\theta_1\dot{\theta}_1^{\,2} \\ L_{x1}\sin\theta_1\dot{\theta}_1^{\,2} \\ (L_1 - L_{x1})\cos\theta_1\dot{\theta}_1^{\,2} + L_{x2}\cos\theta_2\dot{\theta}_2^{\,2} \\ (L_1 - L_{x1})\sin\theta_1\dot{\theta}_1^{\,2} + L_{x2}\sin\theta_2\dot{\theta}_2^{\,2} \\ (L_2 - L_{x2})\cos\theta_2\dot{\theta}_2^{\,2} + L_3\cos\theta_3\dot{\theta}_3^{\,2} \\ (L_2 - L_{x2})\sin\theta_2\dot{\theta}_2^{\,2} + L_3 sin\theta_3\dot{\theta}_3^{\,2} \\ L_{33}\cos(\theta_3 + \theta_{3'})\dot{\theta}_3^{\,2} + L_{x4}cos\theta_4\dot{\theta}_4^{\,2} \\ L_{33}\sin(\theta_3 + \theta_{3'})\dot{\theta}_3^{\,2} + L_{x4}sin\theta_4\dot{\theta}_4^{\,2} \\ (L_4 - L_{x4})\cos\theta_4\dot{\theta}_4^{\,2} + L_{11}sin(\theta_1 + 0.7^\circ)\dot{\theta}_1^{\,2} \\ (L_4 - L_{x4})\sin\theta_4\dot{\theta}_4^{\,2} + L_{11}cos(\theta_1 + 0.7^\circ)\dot{\theta}_1^{\,2} \end{bmatrix}. \quad (8)$$

The acceleration vector is as follows: The external force vector is given as follows:

$$g^{\mathrm{T}} = \begin{bmatrix} 0 & -m_1a_g & 0 & 0 & -m_2a_g & 0 & x_3 & -m_3a_g & \tau & x_4 & -m_3a_g & k\theta_{1\_4} \end{bmatrix} \quad (9)$$

where a_g is the gravitation acceleration.

ORCID iD

Gwang-Pil Jung https://orcid.org/0000-0003-2580-3304

References

An J, Ma X, Lo C H D, Ng W, Chu X and Au K W S 2022 Design and experimental validation of a monopod robot with 3-DoF morphable inertial tail for somersault *IEEE/ASME Trans. Mechatronics* **27** 5072–83

Bai L, Zheng F, Chen X, Sun Y and Hou J 2018 Design and experimental evaluation of a single-actuator continuous hopping robot using the geared symmetric multi-bar mechanism *Appl. Sci.* **9** 13

Batts Z, Kim J and Yamane K 2016a Design of a hopping mechanism using a voice coil actuator: linear elastic actuator in parallel (LEAP) *2016 IEEE Int. Conf. on Robotics and Automation (ICRA)* (IEEE) pp 655–60

Batts Z, Kim J and Yamane K 2016b Untethered one-legged hopping in 3D using linear elastic actuator in parallel (LEAP) *Int. Symp. on Experimental Robotics* (Springer) pp 103–12

Best T L, Hildreth N J and Jones C 1989 Dipodomys deserti *Mamm. Species* **339** 1–8

Chae S-H, Baek S-M, Lee J and Cho K-J 2022 Agile and energy-efficient jumping–crawling robot through rapid transition of locomotion and enhanced jumping height adjustment *IEEE/ASME Trans. Mechatronics* **27** 5890–901

Chen W-H, Misra S, Caporale J D, Koditschek D E, Yang S and Sung C R 2020 A tendon-driven origami hopper triggered by proprioceptive contact detection *2020 3rd IEEE Int. Conf. on Soft Robotics (Robosoft)* (IEEE) pp 373–80

De A and Koditschek D E 2015 The Penn Jerboa: a platform for exploring parallel composition of templates (arXiv:1502.05347)

Flores P and Lankarani H M 2016 *Contact Force Models for Multibody Dynamics* (Berlin: Springer)

Freymiller G A, Whitford M D, Higham T E and Clark R W 2017 Recent interactions with snakes enhance escape performance of desert kangaroo rats (Rodentia: Heteromyidae) during simulated attacks *Biol. J. Linn. Soc.* **122** 651–60

Haldane D W, Plecnik M M, Yim J K and Fearing R S 2016b Robotic vertical jumping agility via series-elastic power modulation *Sci. Robot.* **1** eaag2048

Haldane D W, Plecnik M, Yim J K and Fearing R S 2016a A power modulating leg mechanism for monopedal hopping *2016 IEEE/RSJ Int. Conf. on Intelligent Robots and Systems (IROS)* (IEEE) pp 4757–64

Haldane D W, Yim J K and Fearing R S 2017 Repetitive extreme-acceleration (14-g) spatial jumping with Salto-1P *2017 IEEE/RSJ Int. Conf. on Intelligent Robots and Systems (IROS)* (IEEE) pp 3345–51

Hawkes E W, Xiao C, Peloquin R-A, Keeley C, Begley M R, Pope M T and Niemeyer G 2022 Engineered jumpers overcome biological limits via work multiplication *Nature* **604** 657–61

Hong C, Tang D, Quan Q, Cao Z and Deng Z 2020 A combined series-elastic actuator & parallel-elastic leg no-latch bio-inspired jumping robot *Mech. Mach. Theory* **149** 103814

Jung G-P, Casarez C S, Jung S-P, Fearing R S and Cho K-J 2016 An integrated jumping-crawling robot using height-adjustable jumping module *2016 IEEE Int. Conf. on Robotics and Automation (ICRA)* (IEEE) pp 4680–5

Jung G-P, Casarez C S, Lee J, Baek S-M, YIM S-J, chae S-H, Fearing R S and Cho K-J 2019 Jumproach: a trajectory-adjustable integrated jumping–crawling robot *IEEE/ASME Trans. Mechatronics* **24** 947–58

Jung G-P, Kim J-S, Koh J-S, Jung S-P and Cho K-J 2014 Role of compliant leg in the flea-inspired jumping mechanism *2014 IEEE/RSJ Int. Conf. on Intelligent Robots and Systems* (IEEE) pp 315–20

Kovač M, Schlegel M, Zufferey J-C and Floreano D 2009 A miniature jumping robot with self-recovery capabilities *2009 IEEE/RSJ Int. Conf. on Intelligent Robots and Systems* (IEEE) pp 583–8

Lambrecht B G, Horchler A D and Quinn R D 2005 A small, insect-inspired robot that runs and jumps *Proc. of the 2005 IEEE Int. Conf. on Robotics and Automation* (IEEE) pp 1240–5

Lee D-J and Jung G-P 2020 Snatcher: a highly mobile chameleon-inspired shooting and rapidly retracting manipulator *IEEE Robot. Autom. Lett.* **5** 6097–104

Lee Y-J, Misra S, Chen W-H, Koditschek D E, Sung C and Yang S 2021 Tendon-driven auxetic tubular springs for resilient hopping robots *Adv. Intell. Syst.* **4** 2100152

Li F, Liu W, Fu X, Bonsignori G, Scarfogliero U, Stefanini C and Dario P 2012 Jumping like an insect: design and dynamic optimization of a jumping mini robot based on bio-mimetic inspiration *Mechatronics* **22** 167–76

Li S and Rus D 2019 JelloCube: a continuously jumping robot with soft body *IEEE/ASME Trans. Mechatronics* **24** 447–58

Nguyen Q-V and Park H C 2012 Design and demonstration of a locust-like jumping mechanism for small-scale robots *J. Bionic Eng.* **9** 271–81

Plecnik M M, Haldane D W, Yim J K and Fearing R S 2017 Design exploration and kinematic tuning of a power modulating jumping monopod *J. Mech. Robot.* **9** 011009

Rankin J W, Doney K M and Mcgowan C P 2018 Functional capacity of kangaroo rat hindlimbs: adaptations for locomotor performance *J. R Soc. Interface* **15** 20180303

Ryadchikov I, Sokolov D, Biryuk A, Sechenev S, Svidlov A, Volkodav P, Mamelin Y, Popko K and Nikulchev E 2018 Stabilization of a hopper with three reaction wheels *ISR 2018; 50th Int. Symp. on Robotics* (VDE) pp 1–4

Schwaner M J, Freymiller G A, Clark R W and Mcgowan C P 2021 How to stick the landing: kangaroo rats use their tails to reorient during evasive jumps away from predators *Integr. Comp. Biol.* **61** 442–54

Schwaner M J, Lin D C and McGowan C P 2018 Jumping mechanics of desert kangaroo rats *J. Exp. Biol.* **221** jeb186700

Seok S, Wang A, Otten D and Kim S 2012 Actuator design for high force proprioceptive control in fast legged locomotion *2012 IEEE/RSJ Int. Conf. on Intelligent Robots and Systems* (IEEE) pp 1970–5

Shin W D, Stewart W, Estrada M A, Ijspeert A J and Floreano D 2022 Elastic-actuation mechanism for repetitive hopping based on power modulation and cyclic trajectory generation *IEEE Trans. Robot.* **39** 558–71

Woodward M A and SITTI M 2014 Multimo-bat: a biologically inspired integrated jumping–gliding robot *Int J. Robot. Res.* **33** 1511–29

Yim J K and Fearing R S 2018 Precision jumping limits from flight-phase control in Salto-1P *2018 IEEE/RSJ Int. Conf. on Intelligent Robots and Systems (IROS)* (IEEE) pp 2229–36

Zaitsev V, Gvirsman O, Hanan U B, Weiss A, Ayali A and Kosa G 2015 A locust-inspired miniature jumping robot *Bioinsp. Biomim.* **10** 066012

Zhao J, Xu J, Gao B, Xi N, Cintr´ON F J, Mutka M W and Xiao L 2013 MSU jumper: a single-motor-actuated miniature steerable jumping robot *IEEE Trans.Robot.* **29** 602–14